Seasonal Variability of the Large-Scale Currents near the Coast of the Philippines*

MAX YAREMCHUK AND TANGDONG QU

International Pacific Research Center, University of Hawaii at Manoa, Honolulu, Hawaii

(Manuscript received 21 April 2003, in final form 22 September 2003)

ABSTRACT

The mean seasonal cycle of the western boundary currents in the tropical North Pacific Ocean is studied diagnostically by combining atmospheric climatologies with drifter, satellite altimetry, and hydrographic data in the framework of a simplified numerical model incorporating geostrophy, hydrostatics, continuity, and tracer conservation. The approach enables the authors to diagnose the absolute 3D velocity field and to assess the seasonal cycle of sea surface height (SSH)/total transports. Errors are estimated by considering multiple datasets and averaging over the results of the corresponding diagnostic computations. Analysis shows that bifurcation of the North Equatorial Current (NEC) occurs at 14.3° ± 0.7°N near the Philippine coast. Meridional migration of the NEC bifurcation latitude is accompanied by quantitative changes in the partitioning of the NEC transport between the Kuroshio and Mindanao Current. In February–July, when the NEC transport is 58 ± 3 Sv (Sv ≡ 10^6 m^3 s^{-1}), the Kuroshio transport is 12%–15% higher than the Mindanao Current (MC) transport. In the second half of the annual cycle the situation is reversed: in October the NEC transport drops to 51 ± 2 Sv with the MC transport exceeding the Kuroshio transport by 25%. The net westward transport through the Luzon Strait is characterized by a minimum of 1.2 ± 1.1 Sv in July–September and a maximum of 4.8 ± 0.8 Sv in January–February. A statistically significant correlation is established between the monthly SSH/streamfunction anomalies north of 10°N and the Ekman pumping rate associated with the northeast monsoon developing in the region in October–December. The result provides an indication of the fact that local monsoon is likely to be an important mechanism governing seasonal variation of the NEC partitioning and water mass distribution between the tropical and subtropical North Pacific.

1. Introduction

Low-latitude western boundary currents play an important role in the meridional exchange of mass, heat, and salt in the World Ocean and are believed to be crucial to our understanding of climate dynamics. The Philippine coast in the North Pacific Ocean plays the role of a rigid boundary that splits the wide stream of the North Equatorial Current (NEC) into two parts and produces a complicated circulation pattern as a result of flow interaction with topography (Fig. 1). Seasonal variability of the NEC bifurcation latitude (NECBL) has been studied by Qiu and Lukas (1996), who used a reduced-gravity model forced by Florida State University (FSU) winds to simulate surface circulation in the western tropical Pacific. Metzger and Hurlburt (1996) also observed significant meridional excursions of the NECBL in their numerical simulations and established high correlation of that feature with seasonal changes of the circulation in the South China Sea. Nevertheless, because of limited vertical resolution of these models, seasonal evolution of the 3D circulation remained unexplored. That gap could be filled by analyzing output of high-resolution ocean general circulation models (OGCMs), but, to the best of our knowledge, no attempts have been made so far to study the region east of Philippines with OGCMs. Besides, the results of such analysis could be questionable from a statistical point of view since OGCMs tend to drift away from climatologies in the course of long-term integrations.

Recently Qu et al. (1999) and Qu and Lukas (2003, hereinafter QL03) used an alternative data-oriented approach and carried out a diagnostic study of the ocean state east of Philippines. They used a new climatology of temperature, salinity, and passive tracer fields, compiled for the western tropical Pacific. Relying on a comprehensive water mass analysis and geostrophic velocities relative to 1200 m, QL03 estimated the seasonal cycle of the NECBL and quantified the seasonal oceanic variability in three dimensions. It was shown that the NECBL migration is characterized by an amplitude of 1.2° and a mean position at 15.6°N. The mean NECBL changed considerably with depth, reaching 18°N at 700 m. Below that level it was difficult to trace the NECBL

* International Pacific Research Center/School of Ocean and Earth Science Technology Contribution Number 216/6204.

Corresponding author address: Dr. Max Yaremchuk, International Pacific Research Center, School of Ocean and Earth Science and Technology, University of Hawaii at Manoa, 2525 Correa Road, Honolulu, HI 96822.
E-mail: maxy@soest.hawaii.edu

because of the proximity of the reference quiescent level. Uncertainty of assessment of the near-reference level circulation is the major limitation of the dynamical method used by QL03. Reference level velocity errors may significantly reduce the accuracy of estimation of the NECBL mean position and its seasonal cycle.

In the present study we make an attempt to overcome limitations of the dynamical method by taking into account additional datasets and imposing additional dynamical constraints on the diagnosed flow field. Apart from the hydrographic and wind stress data we utilize surface currents derived from drifting buoys, Ocean Topography Experiment (TOPEX)/Poseidon altimetry, and atmospheric climatologies for heat and freshwater fluxes at the ocean surface. Additional dynamical constraints include continuity and tracer conservation. In addition, hydrographic climatologies are no longer fixed (i.e., assumed to be given with infinite accuracy), but allowed to depart slightly from their gridpoint values and adjust to the structure of the flow field. To perform the analysis, we utilize the 3D variational inversion technique employed by Yaremchuk (2001) for construction of the large-scale circulation in the North Pacific. Errors are estimated by averaging over the ensemble of diagnostic inversions performed with different climatological data and under varying assumptions on the data accuracy.

Besides refining the estimates of NECBL seasonal cycle, we focus on quantifying the partitioning of the NEC transport at the bifurcation point as a feature of major physical importance. Another point of concern is partitioning of the Kuroshio near the northern tip of Luzon (Fig. 1). This feature of circulation is believed to give a significant contribution to the total transport of the Indonesian Throughflow (Wyrtki 1961; Miyama et al. 1995; Lebedev and Yaremchuk 2000) and water mass exchange between the Pacific and Indian Oceans.

The paper is organized as follows. In the next section we provide a brief description of the data and the diagnostic method. Special emphasis is given to the results of preliminary analysis of the drifter and altimetry data since they provide the major information on the barotropic component of the flow. In section 3 we analyze partitioning of the NEC transport near the Philippine coast. Seasonal variability of the Luzon Strait transport and the Kuroshio transport east of Taiwan are considered in section 4. In section 5 we discuss possible mechanisms responsible for partitioning of the NEC and Kuroshio and summarize the results.

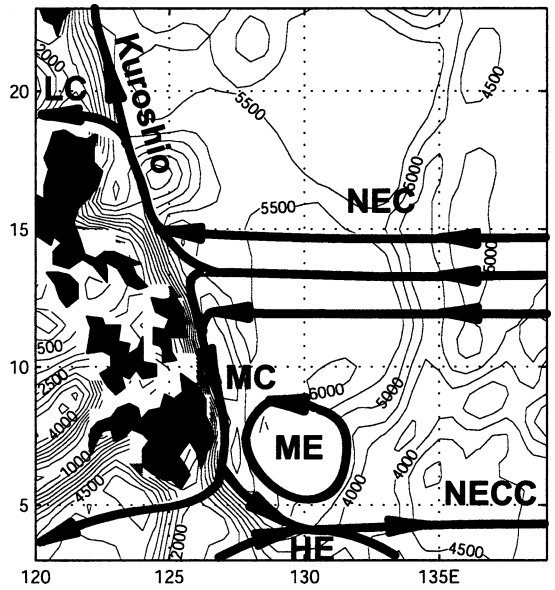

FIG. 1. A schematic representation of the large-scale circulation east of the Philippines. Model domain with bottom topography is shown. Acronyms denote the Luzon Current (LC), the Mindanao Current (MC), the North Equatorial Current (NCC), the North Equatorial Countercurrent (NECC), and the Halmahera (HE) and Mindanao (ME) eddies.

2. Data and method

a. Data

1) HYDROGRAPHY

Our study is based upon two types of gridded temperature and salinity fields. The first one (Fig. 2a) is the *World Ocean Atlas* climatological data (Antonov et al. 1998; Boyer et al. 1998) downloaded from http://www.nodc.noaa.gov/OC5/data_woa.htm, hereinafter referred to as WOA98. The second climatology (Fig. 2b) was compiled by QL03 specifically for the region of the western tropical Pacific. QL03 is based upon the original temperature, salinity, and oxygen profiles from the National Oceanographic Data Center (NODC) World Ocean Database 1998 supplemented by hydrographic data from a number of recent cruises. The data were interpolated along pressure surfaces onto a regular 0.5° grid with a horizontally varying smoothing scale that depended on data density. Prior to interpolation, an extensive quality control was performed to remove profiles with obviously erroneous records. Similar to WOA98, QL03 was compiled for 12 monthly climatologies and the annual mean. Figure 2 gives an idea of the differences between the WOA98 and QL03 climatologies. Rms discrepancies between the corresponding annual means are plotted in Fig. 3 as functions of depth.

2) SURFACE VELOCITIES

Surface velocities were calculated from the trajectories of 567 drifters that moved through the computational domain between January 1979 and December 1999. The data were obtained online at http://www.meds-sdmm.dfo-mpo.gc.ca, the Web site of the Marine Environmental Data Service (Canada). The drifters were drogued between depths 5 and 15 m and therefore sampled the velocity in the surface Ekman layer. Differences in consecutive drifter positions were used to estimate the horizontal distribution of the mean

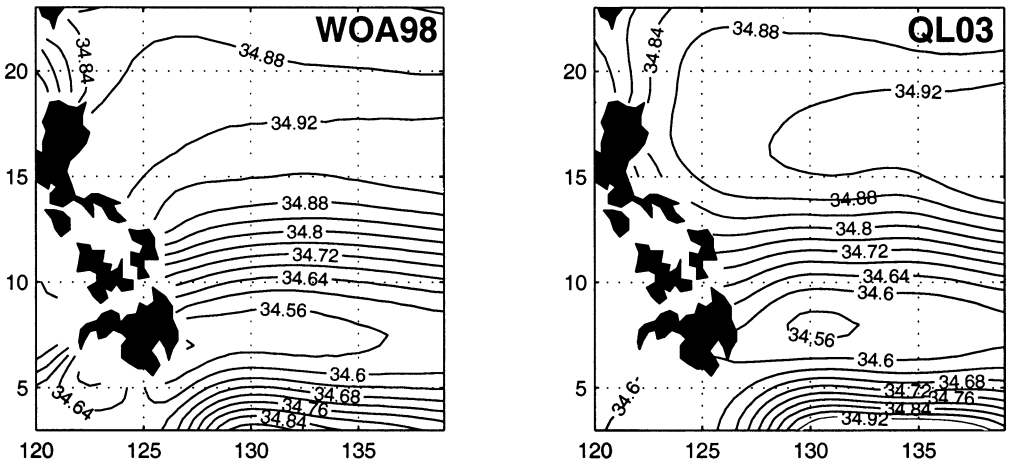

FIG. 2. Annual mean climatological salinity distributions at 250 m. Contour interval is 0.04 psu.

velocity $\mathbf{v}^*$ (Fig. 4). The average time spent by drifters in a 1° grid cell was $t_d = 85.4$ days. The velocity error $\sigma_v(\mathbf{x})$ for a given grid location $\mathbf{x}$ was estimated under the assumptions that (i) individual velocities of different drifters were statistically independent and (ii) decorrelation time scale along a trajectory was $t_d = 5$ days; t_d was determined as the first zero of the velocity autocorrelation function. We found that σ_v was well approximated by the dependence $\sigma_v(\mathbf{x}) = \sqrt{t_d/t(\mathbf{x})} \cdot 28$ cm s^{-1}, where $t(\mathbf{x})$ is the number of days spent by drifters in the grid cell at location $\mathbf{x}$.

3) ALTIMETRY

Drifter velocities cannot provide reliable monthly estimates at every location because of insufficient statistics [annual mean $\sigma_v(\mathbf{x})$ that varies within 2–10 cm s^{-1} should be increased $\sqrt{12} \approx 3.5$ times to obtain monthly error distributions]. This gap can be effectively filled by altimetry, whose accuracy in determination of the monthly mean sea surface height (SSH) *anomalies* is estimated as 2–3 cm (Cheney et al. 1994). On the other hand, altimetry suffers from large geoid errors so that the *absolute* SSH at a given month cannot be determined with an accuracy better than 20–25 cm. To manage the problem we employed drifter velocities for computation of the mean SSH distribution $\overline{\zeta}(\mathbf{x})$. Following the technique proposed by Niiler et al. (2003), we minimized the cost function

$$J = \frac{1}{2}\int_D [g\nabla\overline{\zeta} - f(\mathbf{k}\times\overline{\mathbf{v}}) - \overline{\mathbf{a}}]^2 (f\sigma_v)^{-2}(\mathbf{x})\, dD,$$

with respect to the unknown $\overline{\zeta}$. Here D stands for the 2D rectangular domain representing the ocean surface, $\mathbf{k}$ is the vertical unit vector, g is the acceleration due to gravity, f is the Coriolis parameter, and $\overline{\mathbf{a}}$ denotes the sum of wind-forced and inertial components of acceleration in the horizontal momentum balance. To estimate the first component, we combined wind stress climatologies (see below) with the Ralph and Niiler (1999) parameterization of the Ekman layer. Inertial accelerations were assessed directly from data by taking the differences of consecutive drifter velocities along the trajectories and averaging them over the 1° × 1° grid cells. After that the monthly mean SSH fields were obtained by adding $\overline{\zeta}$ to gridded TOPEX/Poseidon SSH anomalies downloaded from the University of Texas Center of Space Research (ftp.csr.utexas.edu). The resulting monthly mean SSH fields ζ^* (Fig. 5) have an estimated error σ_ζ of 3–6 cm and were used as a weak constraint in the diagnostic calculations described below.

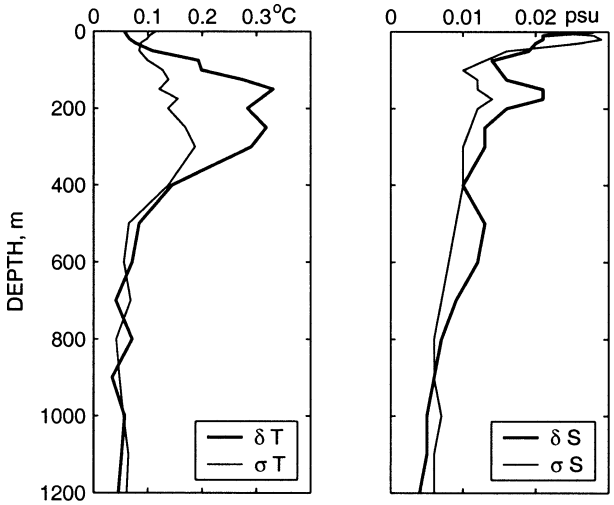

FIG. 3. Vertical profiles of the horizontally averaged rms differences between temperatures (δT) and salinities (δS) of the annual mean WOA98 and QL03 climatologies. Below 1200 m δT and δS were set to the constant values of 0.05°C and 0.003 psu, respectively. Here $\delta T(z)$ and $\delta S(z)$ were used to calculate weighting of the hydrographic data in the diagnostic analysis. Curves labeled by σT and σS demonstrate rms differences in temperature and salinity between the diagnosed ocean state and QL03 climatology.

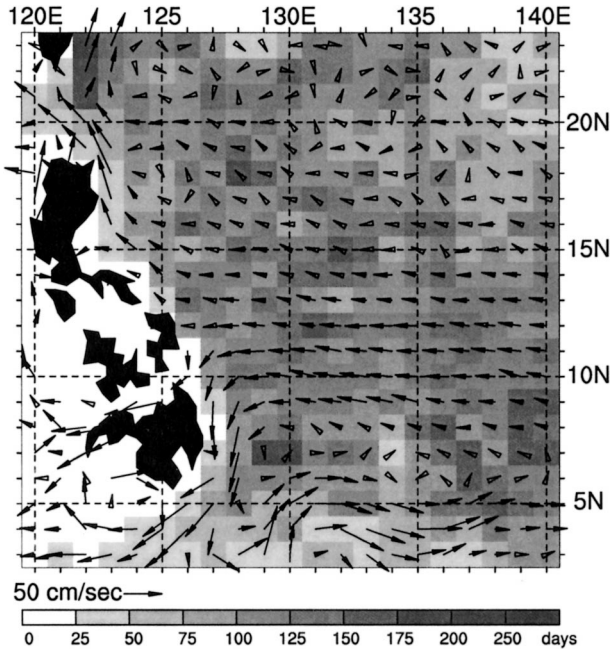

FIG. 4. Annual mean upper layer velocities derived from surface drifters. Shading indicates the total number of days drifting buoys were located in each grid box.

4) ATMOSPHERIC FORCING

Monthly wind stresses $\boldsymbol{\tau}^*$ of Hellerman and Rosenstein (1983), Trenberth et al. (1989), and the National Oceanic and Atmospheric Administration (NOAA) National Centers for Environmental Prediction (NCEP) (http://www.cdc.noaa.gov/Datasets/ncep.marine) were used as the momentum forcing data. Following recommendations of the Tropical Ocean and Global Atmosphere (TOGA) Coupled Ocean–Atmosphere Response Experiment (COARE) numerical experimentation group, the Hellerman and Rosenstein winds were multiplied by the factor of 0.75 (Stockdale et al. 1993). The wind stress error $\sigma_\tau = 0.23$ dyn cm^{-2} was assumed to be independent of horizontal location and was estimated as the rms variance of these wind stress climatologies over the ensemble. Fluxes of heat B_θ^* and freshwater B_S^* were compiled from 1° climatology of Da Silva et al. (1995). In the analysis we assumed that error variances in the ocean–atmosphere fluxes are close to 30% of their spatial variability (Yaremchuk 2001), that is, $\sigma(B_\theta) = 25$ W m^{-2}, $\sigma(B_S) = 32$ cm yr^{-1} for the heat and freshwater fluxes, respectively. Atmospheric products were interpolated on the 0.5° grid using the Gaussian weighting function with a half-width of 2°.

5) OCEAN FLOOR TOPOGRAPHY

Ocean floor topography in Fig. 1 is a smoothed version of the ETOP05 dataset NOAA (1986) (http://web.ngdc.noaa.gov/mgg/global/seltopo.html) adjusted to the 0.5° resolution of the computational grid.

b. Diagnostic method

The general idea of diagnostic analysis in oceanography is to provide an estimate of the ocean state given a set of arbitrary observations. As an example, the traditional dynamical method enables one to compute velocity from temperature and salinity under the assumptions that hydrostatic and geostrophic balances are satisfied exactly and that currents at a certain reference level are negligible.

In the present study we adopt a somewhat more general approach and diagnose oceanic fields under the assumptions of hydrostatic balance, continuity, and conservation of potential temperature θ, salinity S, and momentum. Momentum balance is assumed to be geostrophic except in the thin boundary layers where viscous terms are taken into account. The approach has been used by Yaremchuk (2001) to diagnose the mean large-scale circulation in the North Pacific. A brief description of the method is given below.

We assume a priori that deviations of the diagnosed fields from the data (diagnostic errors) obey Gaussian statistics so that

$$\mathcal{J}_d = \frac{1}{2}\int_{\mathcal{D}} [W_\theta(\theta - \theta^*)^2 + W_S(S - S^*)^2]\, d\mathcal{D} + \int_D [W_\theta^B(B_\theta - B_\theta^*)^2 + W_S^B(B_S - B_S^*)^2 + W_\zeta(\zeta - \zeta^*)^2 + W_\upsilon(\mathbf{v} - \mathbf{v}^*)^2 + W_\tau(\boldsymbol{\tau} - \boldsymbol{\tau}^*)^2]\, dD$$

is the argument of the exponent in the appropriate probability distribution, whereas W_θ, W_S, W_θ^B, W_S^B, W_τ, W_ζ, and W_υ are the inverse error variances σ^{-2} of the corresponding fields, and $\mathcal{D}$ is the 3D diagnostic domain. In addition, oceanic fields are assumed to satisfy the above mentioned set of dynamical constraints, written down in the form of finite-difference equations relating the grid values of the diagnosed fields between each other. Temperature and salinity conservation is treated in the weak form; that is, the corresponding steady-state advection–diffusion balance equations are required to hold within certain errors e_θ and e_S. In contrast to the study of Yaremchuk (2001) who analyzed the long-term mean circulation, we retain temporal derivatives θ_t^* and S_t^* in the tracer balance equations since they are important in diagnosing the seasonal cycle. The temporal derivatives are estimated from the monthly mean climatological fields and treated as the mean values of the errors e_θ, e_S in the steady-state advection–diffusion tracer balance. The ''weak tracer conservation'' is introduced by augmenting the cost function with the term

$$\mathcal{J}_c = \frac{1}{2}\int_{\mathcal{D}} [W_\theta^e(e_\theta - \theta_t^*)^2 + W_S^e(e_S - S_t^*)^2]\, d\mathcal{D}.$$

Here $W_\theta^e(z)$, and $W_S^e(z)$, are the corresponding inverse

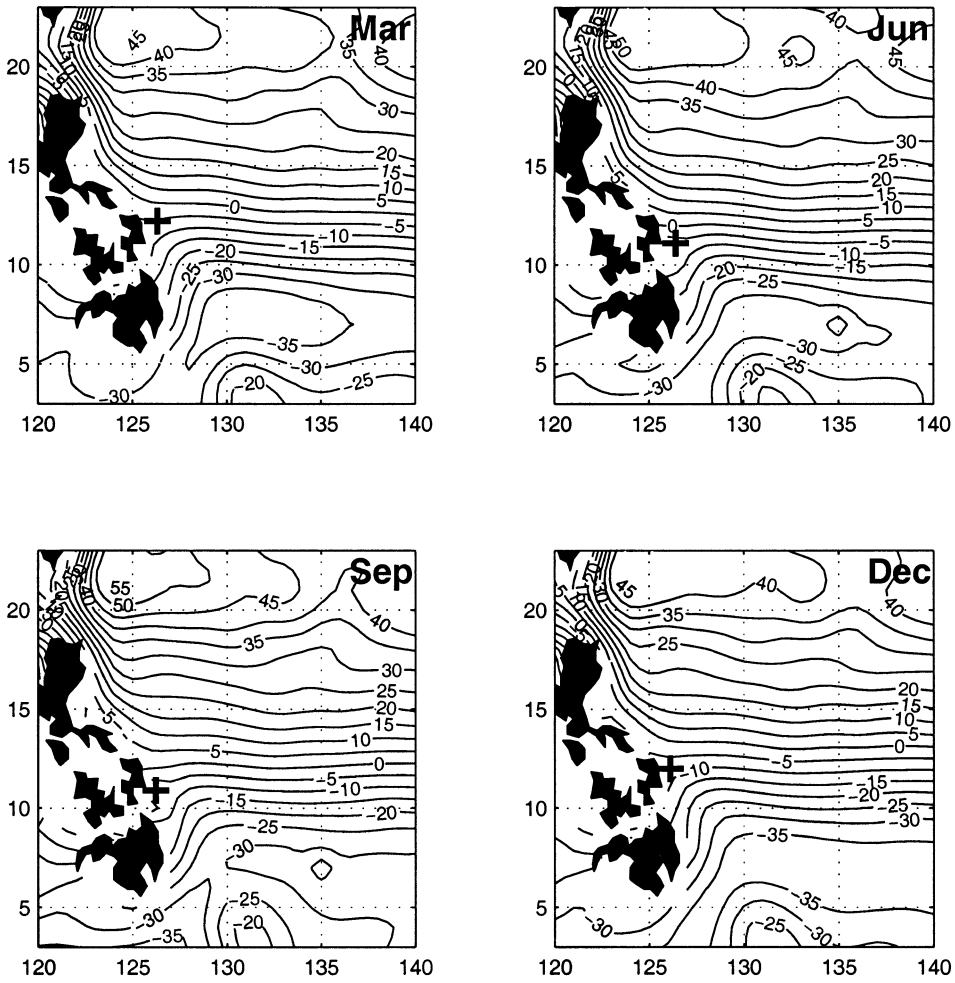

FIG. 5. Monthly sea surface height maps derived from combining drifter velocities with TOPEX/Poseidon data. Contour interval is 5 cm. Boldface cross denotes approximate position of the NEC bifurcation point at the surface.

error variances that were assumed to be inversely proportional to the horizontal variation of potential temperature and salinity divided by T^2, with $T = 60$ days for the monthly, and $T = 1000$ days for the annual mean climatologies. Other terms in the cost function enforce spatial smoothness of the diagnosed fields by penalizing their squared Laplacians:

$$\mathcal{J}_r = \frac{1}{2}\int_{\mathcal{D}} [W_S^s(\Delta S)^2 + W_\theta^s(\Delta\theta)^2]\, d\mathcal{D} + \int_D \left[W_{B_\theta}^s(\Delta B_\theta)^2 + W_{B_S}^s(\Delta B_S)^2 + W_\zeta^s(\Delta\zeta)^2 + W_\tau^s(\Delta\boldsymbol{\tau})^2 + W_\psi^s\left(\Delta\int_{-H}^{0}\mathbf{v}\, dz\right)^2\right] dD,$$

and account for errors $e_w = w - \mathbf{v}|_H \nabla H$ in the integral mass conservation, associated with mass exchange with the bottom boundary layer:

$$\mathcal{J}_w = \frac{1}{2} W^w \int_{z=-H} (e^w)^2\, ds.$$

The "smoothness error variances" $(W^s)^{-1/2}$ were estimated as the rms variations of the corresponding Laplacians of the data fields. The vertical velocity error at the bottom $(W^w)^{-1/2}$ was assumed to have the typical magnitude of the Ekman pumping rate into the bottom boundary layer and was set to 1.5 m yr^{-1} (Yaremchuk 2001).

To diagnose the ocean state, we minimized the quadratic costfunction $\mathcal{J} = \mathcal{J}_d + \mathcal{J}_c + \mathcal{J}_r + \mathcal{J}_w$ with respect to the gridpoint values of θ, S, τ, B_θ, B_S, and ζ. Therefore, the diagnosed fields were found as the most probable in the sense of the prescribed *prior* Gaussian statistics. The dynamically constrained minimization was performed using the adjoint technique.

The studied region covers the area between 3° and 23°N and between 120° and 140°E (Fig. 1). Vertically the domain is divided into 33 levels with separation

varying from 10 m in the upper ocean to 500 m in the deep ocean. The levels coincide with those of the WOA98 climatology. Horizontal resolution of the grid is 0.5°. Subgrid parameterization in the tracer balance equations was set as follows. Vertical diffusion coefficients $K_{\theta,S}$ depended on z as

$$K_{\theta,S} = K^a + K^z \exp(-z^2/z_0^2),$$

with $K^a = 0.4$ cm^2 s^{-1}, $K^z = 10$ cm^2 s^{-1}, and $z_0 = 15$ m. Horizontal diffusion coefficients were 2×10^6 cm^2 s^{-1}.

We performed more than 500 diagnostic runs by varying the data and regularization weights W^s_θ, W^s_S, W^s_ψ in the cost function. The latter were tuned to find an optimal compromise between smoothness and consistency with data. The computations were performed for two temperature/salinity, three wind stress climatologies, and 13 monthly/annual mean datasets. Error bars were computed using the ensembles of the 18 most realistic estimates of the ocean state for each month and for the annual mean. The number of ensemble members (18) is somewhat arbitrary and was limited from above by two factors: available computational resources (each additional ensemble member requires execution of thirteen 3Dvar inversions) and a higher probability of strongly correlated states in a larger ensemble. We assumed that six possible combinations of the data (2 hydrographies $\times$ 3 winds) with three sets of the smoothing weights where enough to produce a representative ensemble.

Since we prescribe relatively small errors to hydrographic data (Fig. 3 curves labeled δT, δS), the diagnosed temperature and salinity fields do not deviate too much from their climatological values (Fig. 3: σT, σS). As a consequence, in the deep open-ocean parts of the basin the vertical velocity shear agrees well with the results of QL03. Near the coastline and steep topographic features bottom relief has a strong impact on both barotropic and baroclinic components of the flow, and relative deviations of the temperature and salinity from their climatological values often reach 30%–50% of their horizontal variance. The absolute velocity field is obtained as a mean-square compromise between fitting the data and satisfying the weak dynamical constraints under the condition that geostrophy, continuity, hydrostatics, and the seawater equation of state are exactly satisfied.

In the following treatment we analyze the results obtained with QL03 climatology since those data proved to be more consistent with dynamics, that is, the values of J were lower after minimizations with QL03 data. The ensemble of diagnosed states involving both QL03 and WOA98 climatologies is utilized for error estimation.

3. Partitioning of the NEC transport

a. Mean state

The annual mean streamfunction of total transport ψ provides a general overview of the circulation in the region (Fig. 6). The pattern was obtained by averaging the diagnostic analyses of QL03 climatology performed with three different wind-forcing datasets. The estimated rms error variance of ψ is 2–4 Sv (Sv $\equiv 10^6$ m^3 s^{-1}).

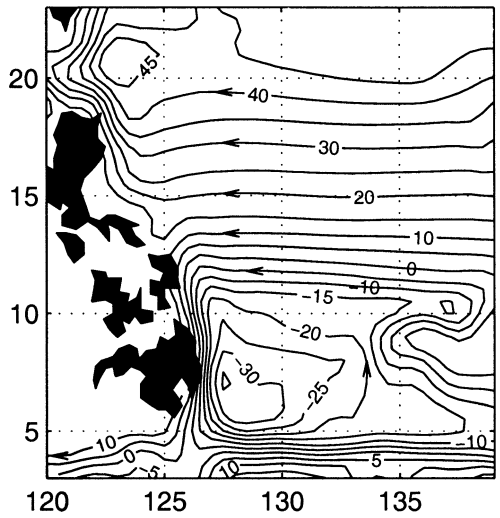

FIG. 6. Annual mean streamfunction of total transport derived from QL03 climatology. Contour interval is 5 Sv.

In the present study we define transports of the Kuroshio and Mindanao Current as the largest differences in ψ between the Philippine coast and along 18.5°N (11°N). The NEC transport is determined as the sum of the MC and Kuroshio transports. Our definition of the MC transport differs from that adopted in earlier diagnostic studies by Wijffels et al. (1995) and Qu et al. (1998), who measured it at 8°N. The reason for assessing of the MC transport at 11°N rather than at 8°N is to exclude the closed cyclonic circulation associated with the Minadanao eddy (Figs. 1 and 6). With this definition, the Kuroshio and MC transports average to 27.6 $\pm$ 2.4 and 30.1 $\pm$ 2.6 Sv, respectively, with the total NEC transport of 57.7 $\pm$ 2.8 Sv. These values are in good correspondence with past observational studies (e.g., Nitani 1972; Lukas et al. 1991; Qu et al. 1998) and recent results of high-resolution OGCM modeling of the region (Y. Kim 2003, personal communication).

As seen from Fig. 6, the mean position of the NEC total transport bifurcation is located near 13°N, that is more than 2° south of the latitude diagnosed by Qu and Lukas (2003), who assumed zero velocities at 1200 m in their diagnostic calculations. This discrepancy is apparently due to significant [O(1 cm s^{-1})] northward velocities that are visible at 1200 m in the latitude band 13°–15°N near the Philippine coast (Fig. 7a). If, instead of diagnosing the NECBL through the total transport pattern in Fig. 6, we define it as the latitude where the mean meridional velocity (averaged vertically over the top 1000 m and zonally within 3° band off the Philippine coast) changes sign, the NECBL will be displaced to 14.3°N. That is still 0.9° to the south of the NECBL

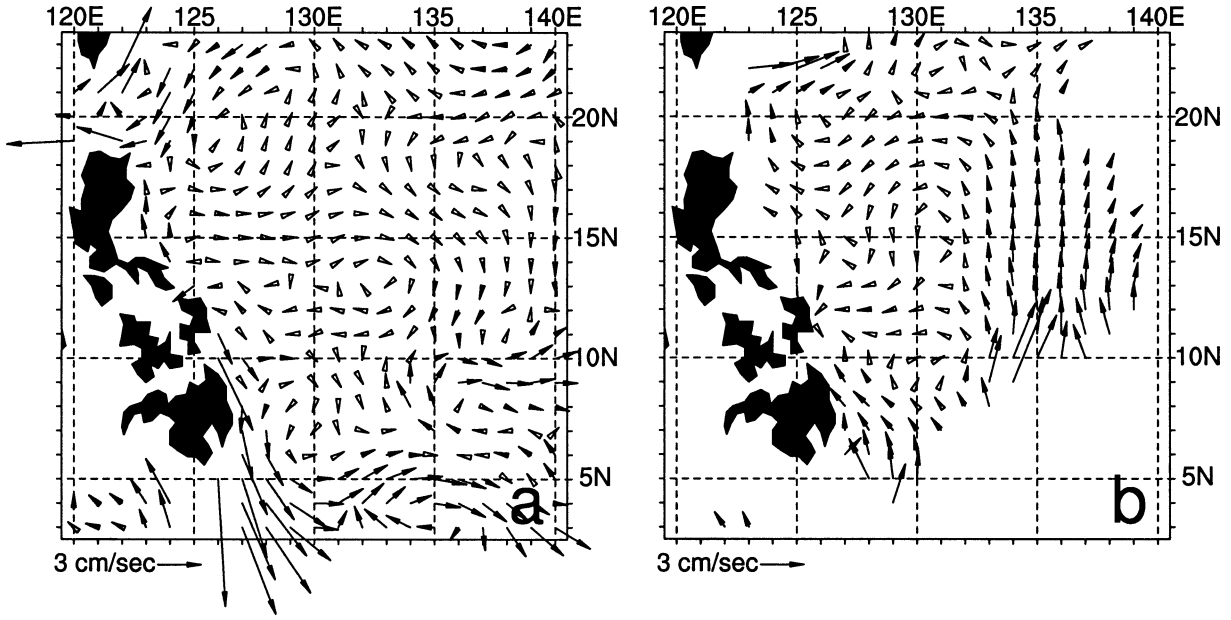

FIG. 7. Annual mean horizontal velocities at (a) 1200 and (b) 5000 m diagnosed from the QL03 climatology.

value of 15.2°N obtained in QL03. It is noteworthy that our estimate 14.3°N for the NECBL is more consistent with the one derived from the simple Sverdrup balance considerations (14.6°N). The obtained estimate of 14.3°N exhibited 0.1° meridional excursions when the averaging region was varied between 900 and 1200 m in depth and 3°–5° in the offshore direction. Larger variations (up to 0.7°) were observed within the ensemble of the 18 optimized annual mean states described in the previous section.

Another important feature of the NEC bifurcation is partitioning of the NEC transport at the Philippine coast. As suggested by the annual mean pattern in Fig. 6, the total volume transport carried by NEC is distributed in an approximately equal proportion between the Kuroshio and Mindanao Current with a slightly larger share of the equatorward flow.

The vertical structure of the annual mean flow is in good qualitative agreement with the results of QL03 in the upper 500 m. Below 500 m an assumption of no motion at 1200 m, adopted in QL03, provides some discrepancies with our results. In contrast to QL03, who diagnosed a southward flow of 0–0.3 cm s^{-1} in the latitude band 15°–20°N beneath 600 m near the Luzon coast (Fig. 8a), our computation reveals a weak (0–1.3 cm s^{-1}) northward pathway for intermediate waters of southern origin at the same location (Fig. 8b). Figure 7a shows that the southward pathway of the North Pacific Intermediate Waters appears to occupy a more easterly position, departing from the Philippines as far as 135°–140°E at 14°–16°N and then returning back to the coast of Mindanao near 10°–12°N. Circulation in the deeper layers is dominated by the northward flows around 135°E and off the Mindanao coast (Fig. 7b), possibly providing a pathway for Antarctic waters into the Northern Hemisphere.

Deep currents did not show any significant evidence of seasonal change, so that all intra-annual variability of circulation was confined to the upper 1000 m.

b. Seasonal variability

Figure 9 shows seasonal evolution of the NECBL obtained as a result of the diagnostic analyses of the monthly QL03 climatologies. Error bars give an idea of the NECBL stability with respect to the variations in the input data (three wind climatologies and QL03/WOA98 hydrographies). Although temporal variations of NECBL are in good agreement with the result of Qu and Lukas (2003), there is a 1.5° southward shift of our estimate. As mentioned in the previous section, the shift occurs because of nonzero alongshore currents at 1200 m, revealed by the dynamically constrained 3D variational analysis. These currents are partly supported by drifter data, which show that the NECBL location at the surface is considerably closer to the equator (Figs. 5 and 9) than the value of 13°N obtained in QL03.

Seasonal variation of the total transports of the Kuroshio at 18.5°N and Mindanao Current at 11°N indicates significant changes in the NEC partitioning (Fig. 10). In February–July Kuroshio transport east of northern Luzon is 1–3 Sv larger than that of the MC, indicating a larger supply of warm water into the Northern Hemisphere. In the summer–autumn season (July–November) the Kuroshio transport drops by 15%, whereas the MC increases in strength from 28 to 34 Sv. Therefore the Kuroshio/MC transport ratio exhibits variations from 1.15 in May to 0.75 in November. With the MC

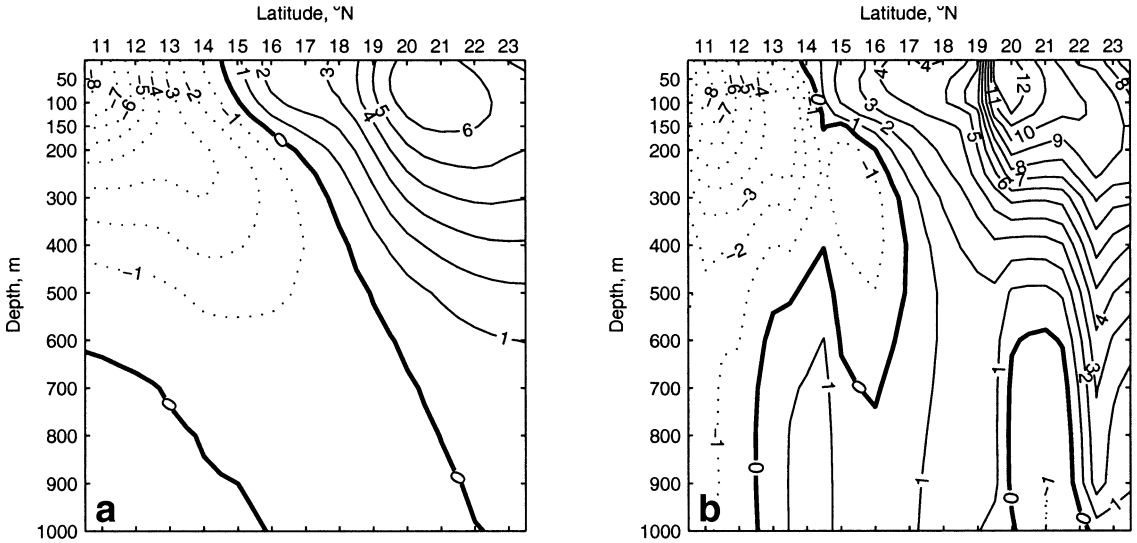

FIG. 8. Annual mean geostrophic velocity (cm s^{-1}) averaged within a 5° longitude band off the Philippine coast: (a) the diagnostic result of Qu and Lukas (2003), and (b) the present study. Positive values indicate northward flow.

transport defined at 8°N and corrected for the annual mean Mindanao eddy transport of 17 Sv, the seasonal cycle remains qualitatively unchanged but much less pronounced because MC transport variations are masked by variations of the intensity of the Mindanao eddy, which tends to be weaker in autumn. In the vertical plane oriented along the Philippine coast we see northward expansion of the MC in winter, accompanied by amplification of the Kuroshio undercurrent visible below 600 m at 20°–22°N (right panel of Fig. 11). Alternatively, the Kuroshio and the deep northward flow under the Mindanao Current (12°–15°N, 600–1000 m) gain maximum strength in late spring (Fig. 11, left panel). The seasonal cycle exposed in Figs. 10–11 appears to be in good qualitative agreement with the earlier observational studies by Qu et al. (1998) and the recent results of high-resolution simulations by Y. Kim (2003, unpublished manuscript). It is also interesting that the Kuroshio transport variations near the northern tip of Luzon (boldface line in Fig. 10) appear to be in qualitative agreement with its variations farther downstream that were obtained from numerical modeling (Kagimoto and Yamagata 1997), observational evidence (Imawaki

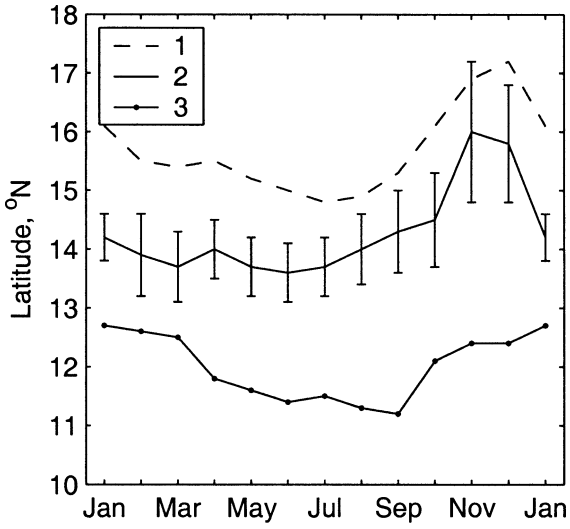

FIG. 9. Seasonal variation of the NECBL determined from the total transport in the upper 1000 m by Qu and Lukas (2003) (curve 1), total transport in the present study (curve 2), and surface geostrophic currents obtained by combining drifter data with TOPEX/Poseidon altimetry (curve 3).

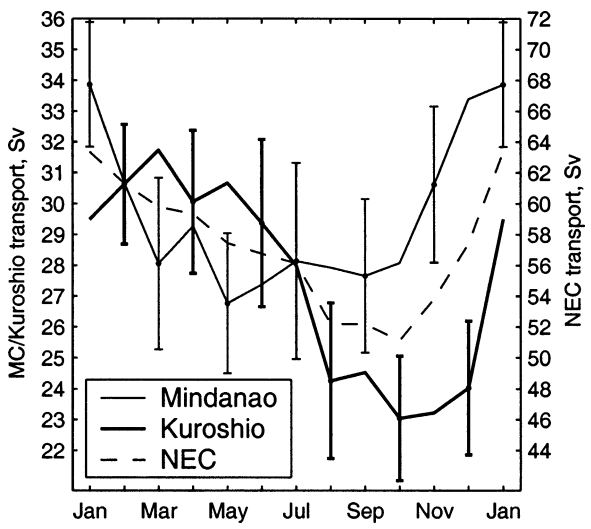

FIG. 10. Seasonal cycle of the Kuroshio transport at 18.5°N and MC transport at 11°N (left *y* axis). Right axis labels variability of the NEC transport shown by the dashed line. Error bars do not change dramatically between the months and are given for every second month to avoid overlapping.

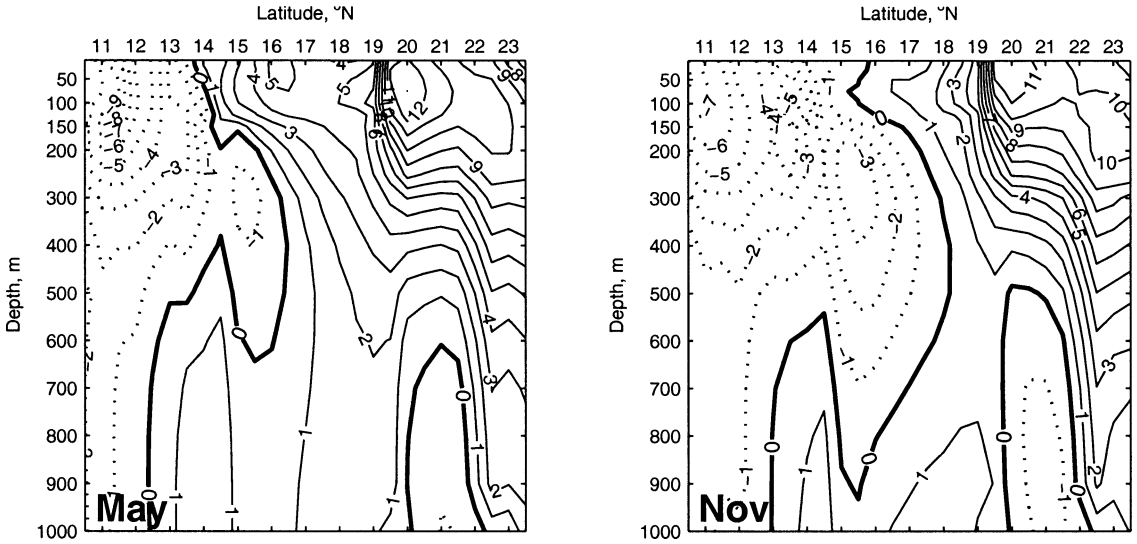

FIG. 11. As in Fig. 8 but for monthly mean velocities in May and Nov.

et al. 2001), and data assimilation (Yaremchuk and Lebedev 2002).

Figure 12 shows the spatial structure of the total transport anomalies. The seasonal cycle starts with the arrival at Luzon of a positive transport anomaly, which displaces the large cyclone (centered at 12°N, 127°E in January) southward. The cyclone subsequently decays off the Mindanao coast in March–July. In late summer and early autumn the cyclonic anomaly emerges again off the coast of Luzon and gains maximum strength in

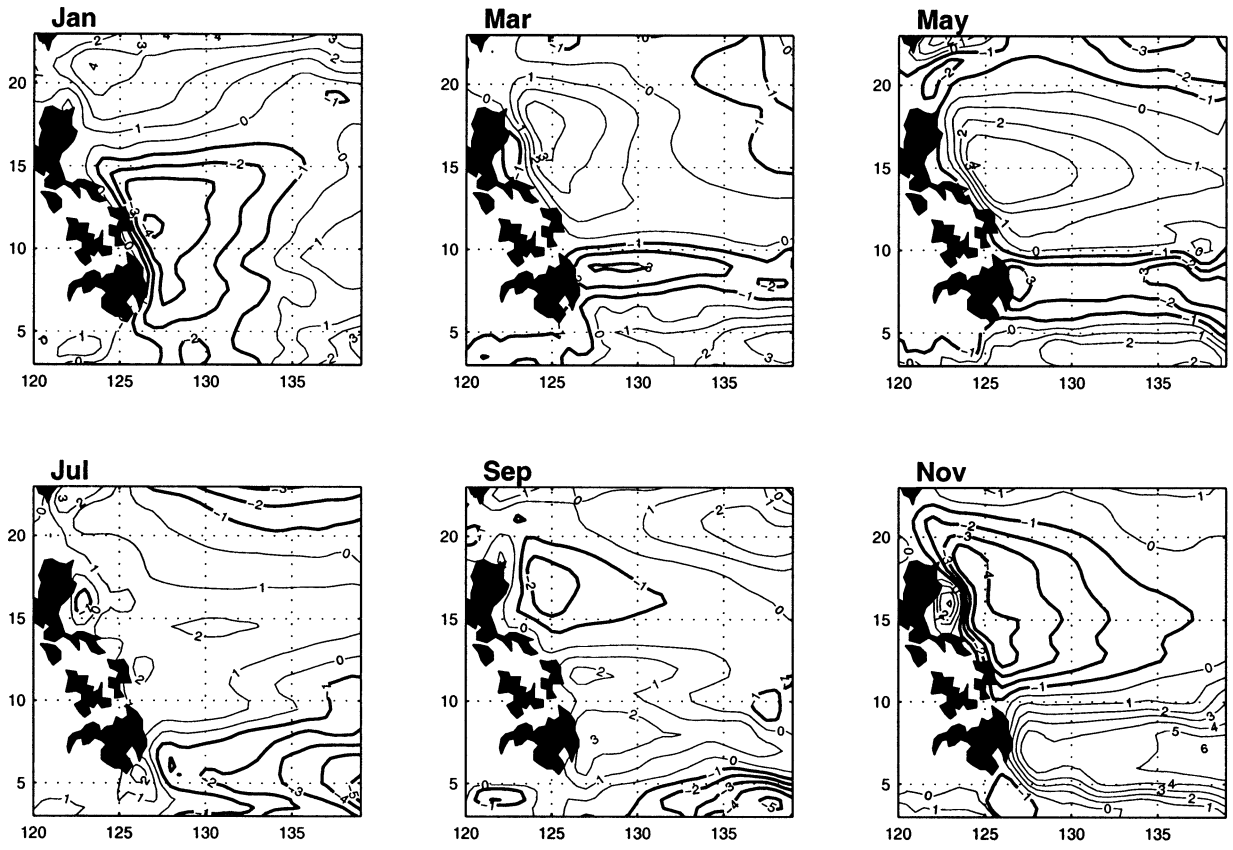

FIG. 12. Annual cycle of the streamfunction anomalies (Sv).

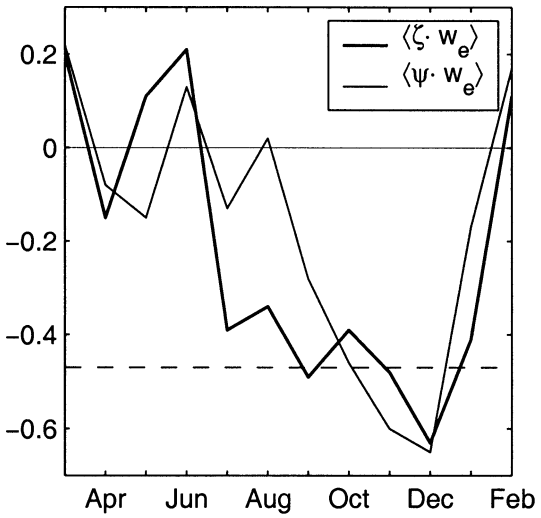

FIG. 13. Seasonal cycle of the correlation between the Ekman pumping rate and the diagnosed SSH (streamfunction) anomalies. For each month averaging has been done within the region north of 13°N. Dashed line shows the 90% confidence limit of nonzero correlation.

November–December, completing the seasonal cycle. We assume that the diagnosed seasonal variability of the transports is primarily driven by the local monsoon winds through Ekman pumping rather than by remote forcing mechanisms. The idea was first put forward by Qu and Lukas (2003), who observed a striking similarity between the meridional excursions of the NECBL and the wind stress curl averaged within 10°–20°N, 120°–140°E.

The major quantitative feature of the local monsoon variability is a strong increase of the positive wind stress curl east of Luzon in October–November, which abruptly decreases in December–January. The associated Ekman pumping rate averaged over three wind stress climatologies appears to be significantly correlated with both ψ and ζ anomalies only in October–January (Fig. 13). Estimates show that September–December monsoon winds east of Luzon yield typical Ekman upwelling rates of 1–3 m day^{-1} and are powerful enough to spin up the anomalous cyclonic circulation east of Luzon (Fig. 12), whose evolution explains the observed partitioning of the NEC transport and NECBL variability. Of course, the real processes governing NEC bifurcation are much more complicated and involve nonlinear, Rossby wave and frictional effects not included in our diagnostic algorithm. Nevertheless we assume that correlations exposed in Fig. 13 provide strong evidence for the fact that the NEC bifurcation is partly governed by the local monsoon.

4. The Luzon Strait throughflow

An important feature of the large-scale circulation around the Philippines is the net transport through the strait between the Luzon and Taiwan (Fig. 1). Dynamically, the Luzon Strait transport (LST) may be governed by a large number of factors, which include large-scale forcing of the Pacific, Kuroshio transport at the northern tip of Luzon, and ''hydrodynamic resistance'' of the numerous outlets from the South China Sea. Strong dependence of the LST on model geometry and friction parameterization in shallow straits makes estimation of the LST by means of numerical modeling a challenging task. For example, Metzger and Hurlburt (1996) obtained an LST ranging from 4 to 12 Sv and noticed its strong dependence on approximation of the topography within the Indonesian seas. Lebedev and Yaremchuk (2000) used 33-level ⅙° OGCM simulations and obtained a seasonal variation of LST between 6.3 Sv in winter and 4.7 Sv in summer. In the recent 6-layer ⅛° simulations of Metzger and Hurlburt (2001) the LST had a mean value of 2.6 Sv in the 1990s and was diagnosed as a highly nondeterministic feature, strongly dependent upon the flow instabilities.

LST estimates derived from observational evidence are also uncertain primarily because of the lack of long-term velocity measurements in the strait. Different authors report mean LST values ranging from 8–10 Sv (Huang et al. 1994) to 0.5–1 Sv (Wyrtki, 1961). In their recent study, Chu and Li (2000) analyzed declassified U.S. Navy archives and obtained a mean LST of 6.5 Sv into the South China Sea with seasonal variation between 1.4 Sv in September and 13.7 Sv in February. Qu et al. (2000) and Qu (2000) analyzed upper-layer hydrographic data in the South China Sea and obtained an annual mean LST of 3–4 Sv with the seasonal cycle characterized by the maximum transport in January–February (5.3 Sv) and minimum (0.2 Sv) in June–July. The most recent observational estimate of LST made by Liang et al. (2003) gives a westward flow of 3 Sv in the upper 300 m.

Our diagnostic computations reveal the LST as a loop current (Fig. 6) with an annual mean inflow of 5.2 $\pm$ 1.4 Sv into the South China Sea along the Luzon coast and a weaker (2.2 $\pm$ 1.2 Sv) outflow along the coast of southern Taiwan. The seasonal variability of its total transport (Fig. 14) is characterized by a minimum of 0.8 $\pm$ 1.1 Sv in August and maximum (4.8 $\pm$ 0.9 Sv) in December–February.

A remarkable feature seen in Fig. 14 is the fast LST growth in autumn, that is, during the period when the Kuroshio near Luzon attains its minimum transport. To a certain extent this could be explained by an extremely strong northeast monsoon developing near the northern tip of Luzon in October–December. Although directly wind-driven circulation does not appear to make a significant contribution to LST, the piling up of water induced by the monsoonal winds is believed to be an important mechanism that changes the pressure difference across the Luzon Strait and eventually affects the LST (e.g., Metzger and Hurlburt 1996; Qu 2000; Lebedev and Yaremchuk 2000). With the diminishing

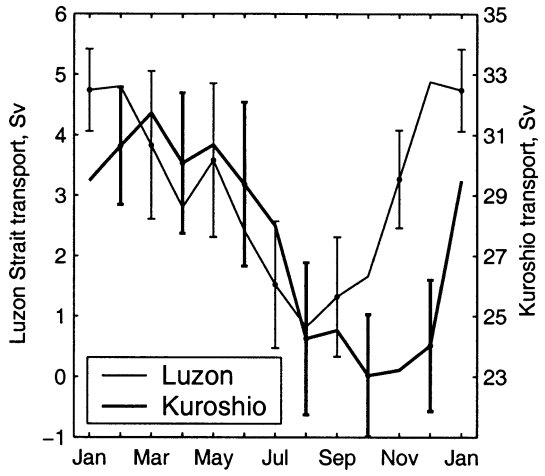

FIG. 14. Seasonal variability of the total transport through the Luzon Strait and of the Kuroshio at 18.5°N. 70% confidence limits are shown.

northwest monsoon in spring, the LST drops toward its seasonal minimum in July–September.

Strong growth of the LST in October–January can also be partly attributed to a nonlinear hysteresis in the Kuroshio's behavior. Sheremet (2001) has shown that an inertial boundary current may leap across a gap in the western boundary (Luzon Strait) when the meridional advection of potential vorticity is strong enough to overpower the β effect, which tends to deviate the current in zonal direction (into the strait). As soon as the current's transport falls below a certain critical value Q_{crit} (depending upon the strait width, β, horizontal and vertical scales of the jet), the current switches into the ''gap penetrating'' regime. Simple estimates show that in our case $Q_{crit} \sim$ 15–20 Sv that is roughly consistent with the diagnosed onset of the gap-penetrating regime (i.e., LST intensification) when the Kuroshio transport approaches its seasonal minimum in October–November (Fig. 14).

Undoubtedly, the described nonlinear mechanism is only one of many possible factors that may influence the dynamics of the Luzon Strait throughflow. Because of possible hysteresis, the LST may also depend on past evolution of the Kuroshio (Farris and Wimbush 1996) and, in particular, on the intra-annual history of the monsoon, which seems to be one of the important driving forces of the seasonal variability in the local large-scale circulation.

5. Discussion and conclusions

We have conducted an extended diagnostic analysis of circulation and transports near the coast of Philippines. Our method incorporates a considerably larger dataset and takes into account more dynamical constraints than the technique applied by Qu and Lukas (2003) to the same region. In particular, we extensively utilized satellite altimetry and drifter velocities to pinpoint the barotropic component of circulation. More accurate prior estimates of the sea surface height were obtained by combining the drifter-referenced mean geostrophic SSH field with SSH anomalies derived from TOPEX/Poseidon altimeter observations. A rigorous error analysis was performed by considering multiple datasets and averaging over the results of the corresponding diagnostic runs.

The approach showed that the position of the NEC bifurcation latitude is farther south than the one obtained from hydrographic data alone. More important, we estimated the seasonal cycle in partitioning of the NEC transport between the Kuroshio and MC at the Philippine coast and assessed seasonal variability of the LST. These two features of local circulation are believed to be important in determining the exchange of waters between the North Pacific subtropical and tropical gyres and between the Pacific and Indian Oceans. The hypothesis of Qu and Lukas (2003) on the importance of local monsoon forcing in distributing the NEC water masses between the Tropics and subtropics is further confirmed here by establishing significant correlations between the streamfunction anomalies and the Ekman pumping associated with the Asian winter monsoon.

The major results of the study can be summarized as follows.

1) The mean position of the NEC bifurcation latitude is 14.3° ± 0.7°N, which is 0.9° farther south than the value given by QL03. In November–December the NECBL reaches its northernmost position of 15.8° ± 1.3°N. In summer the NECBL is located at 13.8° ± 0.5°N.
2) In the annual mean the NEC splits in approximately equal proportion between the Kuroshio (27.6 ± 2.4 Sv) and Mindanao (30.1 ± 2.6 Sv) currents. However, in February–July the Kuroshio transport is 1–3 Sv more than that of MC, indicating a larger supply of warm water into the Northern Hemisphere. In the rest of the year the situation is reversed: the Kuroshio transport drops from 28 ± 2.3 Sv to 23 ± 2 Sv, whereas the MC increases in strength from 28 to 34 Sv.
3) A statistically significant correlation between the SSH/streamfunction anomalies and the Ekman pumping rate associated with the northeast monsoon is detected in November–January. This suggests that the Asian monsoon is the primary mechanism governing seasonal variation in the distribution of waters between the Tropics and subtropics.
4) The total transport through the Luzon Strait has a mean value of 3 ± 1 Sv with seasonal variation from 0.8 ± 1.1 Sv in August to 4.8 ± 0.9 Sv in December–February. Comparison of the LST variability with the Kuroshio transport east of Luzon indicates potential importance of the inertial effects in the dynamics of the Kuroshio penetration into the South China Sea.

The study has also shown that the assumption of no motion at 1200 m is a good proxy for correct estimation of the geostrophic currents in most of the studied region. However, near the coast of Philippines the assumption is less accurate; and the along-coastal currents at 1200 m cause substantial changes in the location of such a sensitive feature as the NECBL. Additional computations have shown that it is impossible to find a notably better level of no motion than 1200 m: reference levels in the depth range between 1 and 2 km gave approximately the same (1–4 cm s^{-1}) velocity errors along the Philippine coast, which seems to be large for quantitative studies of the NECBL. It is also necessary to note that eddy activity near the coast of Philippines may contribute substantially by eddy-driven mass and property fluxes that may be comparable with the diagnosed transport anomalies. To take the eddies into account and diagnose the physical mechanisms that drive local variability, we need to employ a 4D data assimilation technique constrained by a higher-resolution primitive equation model. That will be the subject of future research.

Acknowledgments. This study was supported by the Frontier Research System for Global Change through its sponsorship of the International Pacific Research Center. Author T. Qu was also supported by the National Science Foundation Grant OCE00-95906. The Center for Space Research of the University of Texas at Austin is acknowledged for providing the preprocessed TOPEX/Poseidon data. Helpful discussions with Dr. H. Mitsudera, Dr. T. Jensen, and Dr. J. Potemra are also acknowledged.

REFERENCES

Antonov, J., S. Levitus, T. P. Boyer, M. Conkright, T. O'Brien, and C. Stephens, 1998: *Temperature of the Pacific Ocean.* Vol. 2, *World Ocean Atlas 1998*, NOAA Atlas NESDIS 28, 166 pp.

Boyer, T. P., S. Levitus, J. Antonov, M. Conkright, T. O'Brien, and C. Stephens, 1998: *Salinity of the Pacific Ocean.* Vol. 5, *World Ocean Atlas 1998*, NOAA Atlas NESDIS 31, 166 pp.

Cheney, R., L. Miller, R. Agreen, N. Doyle, and J. Lillibridge, 1994: TOPEX/POSEIDON: The 2-cm solution. *J. Geophys. Res.,* **99** (C12), 24 555–24 563.

Chu, P., and R. Li, 2000: South China Sea isopycnal-surface circulation. *J. Phys. Oceanogr.,* **30,** 2419–2438.

Da Silva, A., C. C. Young, and S. Levitus, 1995: *Atlas of Surface Marine Data.* NOAA Atlas NESDIS 6, National Oceanographic Data Center, Silver Spring, MD, 83 pp.

Farris, A., and M. Wimbush, 1996: Wind-induced Kuroshio intrusion into the South China Sea. *J. Oceanogr.,* **52,** 771–784.

Hellerman, S., and M. Rosenstein, 1983: Normal monthly wind stress over the world ocean with error estimates. *J. Phys. Oceanogr.,* **13,** 1093–1104.

Huang, Q. Z., W. Z. Wang, Y. S. Li, and C. W. Li, 1994: Current characteristics of the South China Sea. *Oceanology of China Seas,* Z. Di, L. Yuan-Bo, and Z. Cheng-Kui, Eds., Kluwer Academic, 113–122.

Imawaki, S., H. Uchida, H. Ichikawa, M. Fukasawa, S. Umatani, and ASUKA Group, 2001: Satellite altimeter monitoring the Kuroshio transport south of Japan. *Geophys. Res. Lett.,* **28,** 17–29.

Kagimoto, T., and T. Yamagata, 1997: Seasonal transport variations of the Kuroshio: An OGCM simulation. *J. Phys. Oceanogr.,* **27,** 403–418.

Lebedev, K., and M. Yaremchuk, 2000: A diagnostic study of the Indonesian Throughflow. *J. Geophys. Res.,* **105** (C5), 11 243–11 258.

Liang, W.-D., T. Y. Tang, Y. J. Yang, M. T. Ko, and W.-S. Chuang, 2003: Upper-ocean currents around Taiwan. *Deep-Sea Res.,* **50B,** 1085–1105.

Lukas, R., E. Firing, P. Hacker, P. L. Richardson, C. A. Collins, R. Fine, and R. Gammon, 1991: Observations of the Mindanao Current during the Western Equatorial Pacific Ocean Circulation Study. *J. Geophys. Res.,* **96,** 7089–7104.

Metzger, E. J., and H. E. Hurlburt, 1996: Coupled dynamics of the South China Sea, the Sulu Sea, and the Pacific Ocean. *J. Geophys. Res.,* **101,** 12 331–12 352.

——, and ——, 2001: The nondeterministic nature of Kuroshio penetration and eddy shedding in the South China Sea. *J. Phys. Oceanogr.,* **31,** 1713–1732.

Miyama, T., T. Awaji, K. Akimoto, and N. Imasato, 1995: Study of seasonal transport variations in the Indonesian seas. *J. Geophys. Res.,* **100,** 20 517–20 541.

Niiler, P. P., N. A. Maximenko, G. G. Panteleev, T. Yamagata, and D. B. Olson, 2003: Near-surface dynamical structure of the Kuroshio Extension. *J. Geophys. Res.,* **108,** 3193, doi:10.1029/2002JC001461.

Nitani, H., 1972: Beginning of the Kuroshio. *Kuroshio: Its Physical Aspects,* H. Stommel and K. Yoshida, Eds., University of Tokyo Press, 129–163.

NOAA, 1986: ETOP05 digital relief of the surface of the earth data announcement. NOAA Tech. Rep. 86-MGG-07, National Geophysical Data Center, Washington, DC, 2 pp.

Qiu, T., and R. Lukas, 1996: Seasonal and interannual variability of the North Equatorial Current, the Mindanao Current, and the Kuroshio along the Pacific western boundary. *J. Geophys. Res.,* **101,** 12 315–12 330.

Qu, T., 2000: Upper-layer circulation in the South China Sea. *J. Phys. Oceanogr.,* **30,** 1450–1460.

——, and R. Lukas, 2003: On the bifurcation of the North Equatorial Current in the Pacific. *J. Phys. Oceanogr.,* **33,** 5–18.

——, H. Mitsudera, and T. Yamagata, 1998: On the western boundary currents in the Philippine Sea. *J. Geophys. Res.,* **103,** 7537–7548.

——, ——, and ——, 1999: A climatology of the circulation and water mass distribution near the Philippine coast. *J. Phys. Oceanogr.,* **29,** 1488–1505.

——, ——, and ——, 2000: Intrusion of the North Pacific waters in the South China Sea. *J. Geophys. Res.,* **105** (C3), 6415–6424.

Ralph, E. A., and P. P. Niiler, 1999: Wind-driven currents in the tropical Pacific. *J. Phys. Oceanogr.,* **29,** 2121–2129.

Sheremet, V., 2001: Hysteresis of a western boundary current leaping across a gap. *J. Phys. Oceanogr.,* **31,** 1247–1259.

Stockdale, T., D. Anderson, M. Davey, P. Delecluse, A. Kattenberg, Y. Kitamura, M. Latif, and T. Yamagata, 1993: Intercomparison of tropical ocean GCMs. WMO Tech. Doc. 545, WCRP-79, Geneva, Switzerland, 90 pp.

Trenberth, K. E., J. G. Olson, and W. G. Large, 1989: A global ocean wind stress climatology based on ECMWF analyses. NCAR Tech. Note NCAR/TN-338 + STR, 93 pp.

Wijffels, S., E. Firing, and J. Toole, 1995: The mean structure and variability of the Mindanao Current at 8°N. *J. Geophys. Res.,* **100,** 18 421–18 435.

Wyrtki, K., 1961: Physical oceanography of the southeast Asian waters: Scientific results of marine investigations of the South China Sea and Gulf of Thailand, 1959–1961. Naga Rep. 2, Scripps Institute of Oceanography, 195 pp.

Yaremchuk, M. I., 2001: A reconstruction of large scale circulation in the Pacific Ocean north of 10°N. *J. Geophys. Res.,* **106** (C2), 2331–2344.

——, and K. Lebedev, 2002: Inverse modeling of intra-annual variability in the subtropical North Pacific. *J. Phys. Oceanogr.,* **32,** 2725–2741.